Electronically Reconfigurable Reverberation Chambers

Jon W. Wallace, Rashid Mehmood, and Michael A. Jensen
Brigham Young University, USA
E-mail: wall@ieee.org, r.mehmood@ieee.org, jensen@byu.edu

***Abstract*—The idea of an electronically reconfigurable reverberation chamber (ERRC) is introduced, whose purpose is to support over-the-air (OTA) testing in a compact and cost-effective way. In contrast to mechanically stirred chambers, the ERRC operates by randomly varying reconfigurable loads placed on the walls of the chamber. An idealized two-dimensional structure is analyzed revealing that the fading distribution, spatial correlation, frequency selectivity, and multipath directivity can be controlled by proper specification of the random loads.**

I. Introduction

As wireless devices become more sophisticated, exploiting multiple polarizations and multiple spatial degrees of freedom, the ability to characterize and assess relative performance in a repeatable way becomes increasingly difficult. Theoretically, the performance of a multiport antenna system can be characterized separately from higher-level signal processing, modulation, and coding, but doing so in a device- and algorithm-independent way is very difficult.

In contrast to isolated antenna system characterization, over-the-air (OTA) testing measures the performance of complete end-to-end communications in a controlled propagation environment. One method for OTA testing is demonstrated in [1–3], where the device under test (DUT) is surrounded by an array of antennas in an anechoic chamber, allowing several realistic multipath environments to be simulated in a repeatable way. A more economical and compact method is to use a mode stirred reverberation chamber [4, 5], also allowing repeatable end-to-end testing of devices. However, the ability to control the detailed propagation parameters for reverberation chambers is often limited.

Inspired by developments in acoustic wave field synthesis, this paper explores the idea of an electronically reconfigurable reverberation chamber (ERRC). The ERRC can be seen as a device that would allow detailed specification of wave-field parameters, similar to that of an anechoic chamber OTA setup, but realized in a more cost-effective and compact chamber. This initial study explores the potential of the ERRC concept by analyzing an idealized two-dimensional chamber, illustrating that fading distribution, spatial correlation, frequency selectivity, and directional channel response can be controlled to generate useful synthetic propagation channels.

II. Idealized Chamber Topology

This work considers a circular two-dimensional chamber, but the idea can be naturally extended to three-dimensional operation. The idealized chamber is depicted in Figure 1, consisting of an outer wall whose surface is densely covered with radiating antennas that are accessible at external ports. Exciting these ports generates waves that radiate into the chamber, generating a desired wave field at the device under test (DUT). Additionally, loads can be placed at the ports to absorb outgoing waves that are scattered by the DUT.

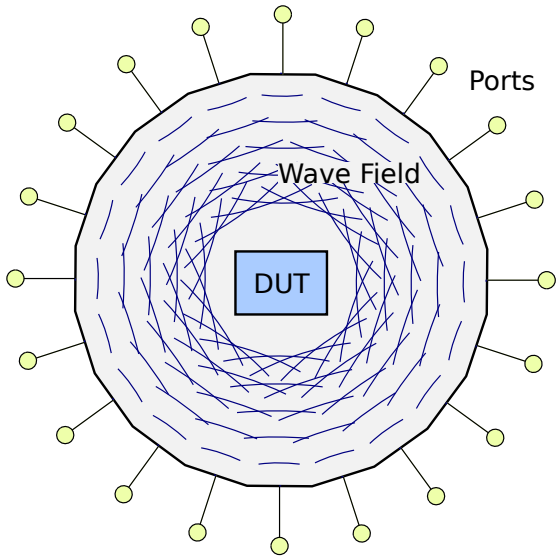

Fig. 1. Idealized two-dimensional chamber.

In this work, the idealized chamber is efficiently modeled using the surface-based method-of-moments framework presented in [6], which was applied for on-body propagation. In this two-dimensional framework, the TM_z fields in the chamber are completely determined by E_z and $\partial E_z/\partial n$ on the outer boundary, where

$$E_z(x,y) = \sum_{m=1}^{M} a_m f_m(x,y) \tag{1}$$

$$\frac{\partial E_z(x,y)}{\partial n} = \sum_{m=1}^{M} b_m f_m(x,y), \tag{2}$$

a_m and b_m are unknown coefficients, $f_m(x,y)$ is a pulse basis function for the mth surface element, and $\hat{n}$ is the outward surface normal. Applying the moment method, a system of equations for the chamber is found as

$$[\mathbf{I} + \mathbf{Q}]\mathbf{a} = \mathbf{S}\mathbf{b}, \tag{3}$$

where $\mathbf{I}$ is the identity matrix and expressions for the matrices $\mathbf{Q}$ and $\mathbf{S}$ are given in [6].

We next develop an equivalent-circuit model of this system. Denoting tangential electric and magnetic field intensities at

978-88-907018-4-9/14/$31.00 ©2014 IEEE

the boundary as E_0 and H_0, respectively, and considering propagation at a single planar boundary reveals

$$E_0 = E_z \qquad \triangleq v \tag{4}$$

$$H_0 = \frac{1}{jk_0\eta_0}\frac{\partial E_z}{\partial n} \qquad \triangleq i, \tag{5}$$

where k_0 and η_0 are the wavenumber and intrinsic impedance of free space, and v and i denote equivalent voltage and current quantities. Combining this result with (3), we obtain

$$\underbrace{[\mathbf{I}+\mathbf{Q}]^{-1}\mathbf{S}(jk_0\eta_0)}_{\mathbf{Z}}\mathbf{i} = \mathbf{v}, \tag{6}$$

where $\mathbf{Z}$ is equivalent impedance matrix of the system. The matrix equation (6) allows the chamber to be analyzed with equivalent-circuit techniques, where sources and loads can be placed on the ports, and the current and voltage vectors $\mathbf{i}$ and $\mathbf{v}$ can be found. Interior fields of the chamber can then be found by solving for $\mathbf{a}$ and $\mathbf{b}$ and applying [6]

$$E_z(x,y) = -\mathbf{Q}(x,y)\mathbf{a} + \mathbf{S}(x,y)\mathbf{b}. \tag{7}$$

Although in this work an idealized two-dimensional ERRC is considered, where fields on the boundary are directly excited at idealized ports, a practical implementation would be possible by using conformal slots and/or patches on the wall of a three-dimensional structure. Practical ERRC implementations are to be considered in future work.

III. Electromagnetic Wave-field Synthesis

A straightforward but costly way to use the chamber is to excite each port of the chamber with an independent source. To provide absorption of waves scattered by a DUT, the sources should have an embedded impedance that absorbs signals flowing out the port. In initial investigations, we have found that terminating the ports with the free-space wave impedance (377 Ω) provides reasonable absorption of outgoing waves.

Figure 2 illustrates how a multipath wave field can be almost exactly realized using this technique. Here the chamber has a diameter of 4λ, where λ is the free space wavelength, and the outer boundary is excited at 101 equally spaced ports, where each port is driven with a voltage source having an internal impedance of 377 Ω. The desired wave field was generated by superimposing 20 plane wave components, each having Rayleigh amplitude, uniform phase, and uniform arrival angle. The source voltages at the ports are then specified by computing the desired field in an inner 2λ diameter control region in the middle of the chamber and inverting the equivalent-circuit model to find the required currents (and therefore source voltages) at the boundary. As shown in the figure, the complicated incident wave field is almost exactly reconstructed using this technique, which should be expected based on Huygens' principle.

Although the independent excitation of each port provides nearly arbitrary specification of incident fields in the chamber, a more cost-effective method is to use the chamber in a manner similar to mode-stirred reverberation chambers. However, instead of using mechanical movement of scatterers in the chamber, reconfigurable loads are used at the boundary ports to provide control over incident fields in the chamber, which is the idea of an ERRC.

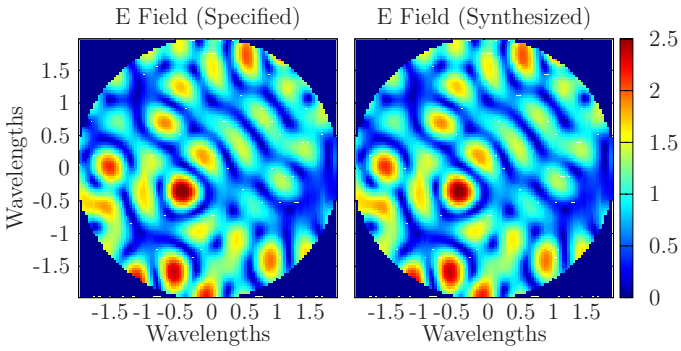

Fig. 2. Synthesis of a multipath wave field using the idealized two-dimensional chamber.

IV. Synthesis of Channel Fading

This section illustrates how channel fading can be simulated using a simpler structure than one where sources are placed on all ports. The same 4λ chamber is considered, but in this case with only 32 ports, as depicted in Figure 3. The ERRC is realized by driving only four ports with active sources with constant amplitude and phase, while terminating the other 28 ports with lossy reconfigurable elements (REs).

A. Generation of Rayleigh Fading

First we consider the possibility of generating close to Rayleigh fading by attempting to make the fields in the chamber as random as possible. For this case, the voltages of the active sources are chosen to be $\mathbf{v}_s = [1 \;\; j \;\; -1 \;\; -j]^T$, where $j = \sqrt{-1}$, and a source impedance of $R_{s,i} = 377\ \Omega$. The impedance of the ith RE is given by $Z_i = R_i + jX_i$, where a constant resistance of 34 Ω is assumed and $X_i \sim \mathcal{U}(-500\ \Omega, 500\ \Omega)$, where $\mathcal{U}(x_1, x_2)$ denotes a uniform distribution on the interval $[x_1, x_2]$. The statistics of the fading in the chamber are analyzed by storing the fields at 24 sample points separated by 0.04λ placed along the line L in Figure 3.

A simulation of 10^4 random realizations is performed, where only the RE reactances are randomly varied as described above. Figures 4 and 5 plot the amplitude/phase probability density functions (pdfs) at the center sample point and the average correlation coefficient along the line L, respectively. As can be seen, the statistics are close to an ideal Rayleigh distribution. Further improvement and fitting of other distributions is possible by more careful selection of the RE impedances, as described below.

B. Fading Distribution Optimization

Next we illustrate how the parameters of the ERRC port terminations can be controlled in order to generate a particular channel fading environment inside the chamber. In this study, we consider optimization of the following parameters:

1) The source excitation voltage vector $\mathbf{v}_s$, whose elements can be arbitrary complex values (amplitude and phase) under the constraint $0 \leq |v_{s,i}| \leq 1$.
2) The constant resistance R_0 of the RE impedances ($R_i = R_0$), where the constraint $R_0 \in [10, 145]\ \Omega$ is assumed
3) The endpoints $X_{\min}$ and $X_{\max}$ of the uniform distribution used for the RE reactances, where

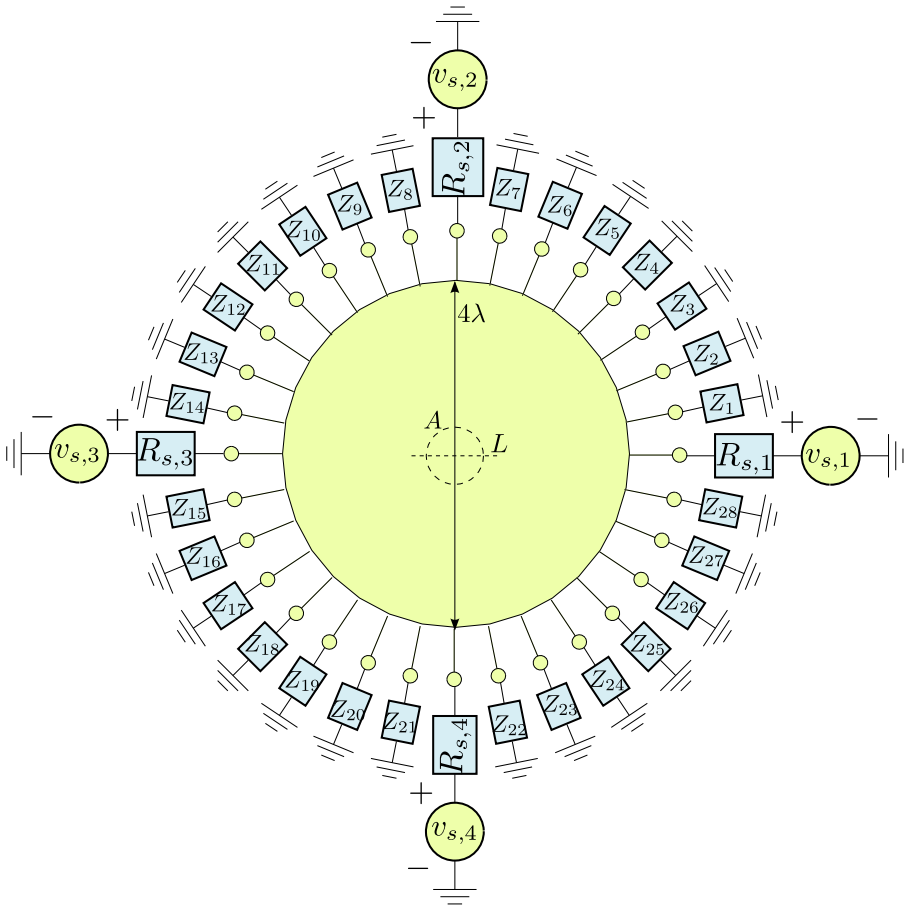

Fig. 3. Chamber topology used for fading studies, where four ports are driven with active sources and the remaining 24 ports are terminated with reconfigurable impedances.

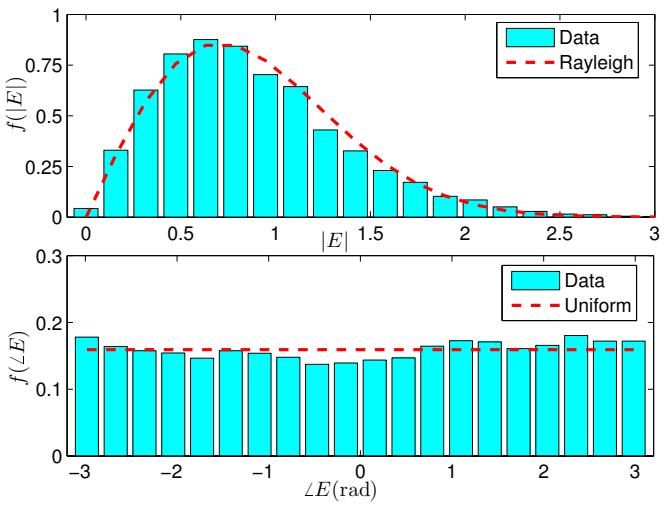

Fig. 4. Amplitude and phase pdfs of the field sampled at the center of the chamber for uniform random loads at the reconfigurable ports.

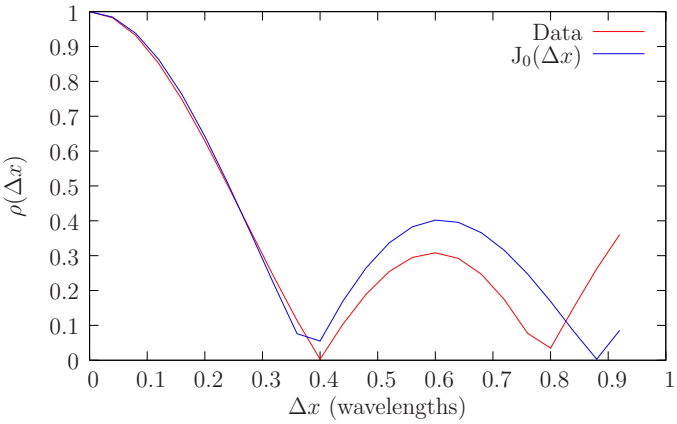

Fig. 5. Average correlation coefficient of field sample points along the center line of the chamber, compared with Jakes' model.

$X_i \sim \mathcal{U}(X_{\min}, X_{\max})$. The bounds $X_{\min}, X_{\max} \in [-2\eta_o, 2\eta_o]$ and $X_{\min} < X_{\max}$ are assumed.

These parameters are collected into the 11-element vector

$$\mathbf{w} = [|\mathbf{v}_s^T| \ \angle\mathbf{v}_s^T \ R_0 \ X_{\min} \ X_{\max}]^T, \tag{8}$$

where optimization of the parameters is performed using a genetic algorithm (GA) using the fitness function

$$F(\mathbf{w}) = -\max_i |f_{\text{ideal}}(x_i) - f_{\text{actual}}(x_i|\mathbf{w})|^2, \tag{9}$$

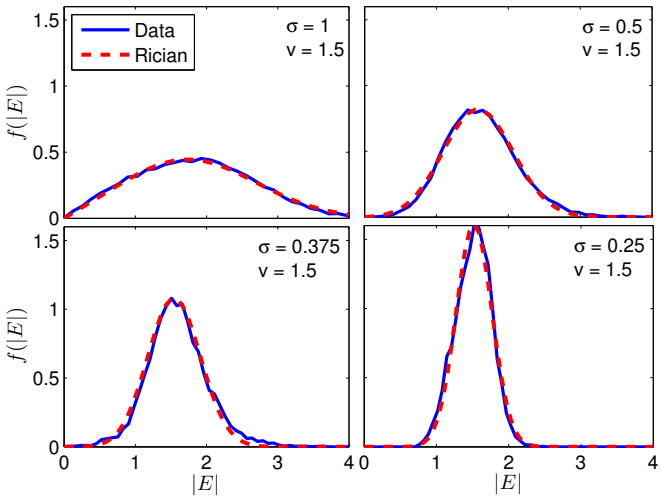

Fig. 6. Amplitude pdfs of the field sampled at the center of the chamber for uniform RE reactances, where in each case the distribution parameters are optimized for a specific value of σ and ν.

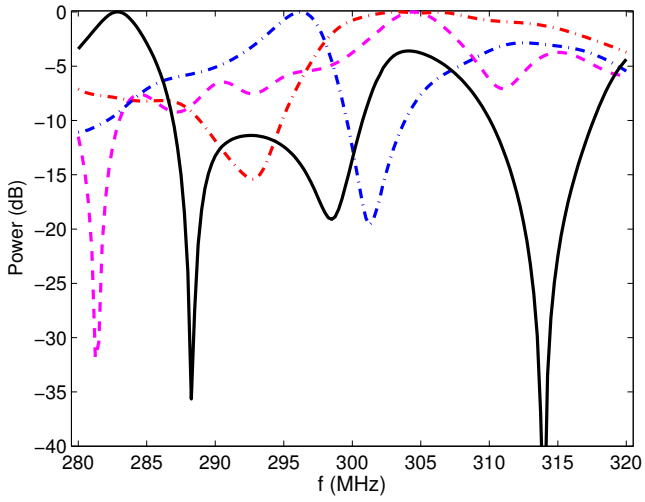

Fig. 7. Power versus frequency for 4 different realizations of the RE reactances, where the field was sampled in the middle of the chamber.

which minimizes the maximum squared error between the ideal and actual pdfs.

The GA starts with a randomization phase having an initial population of $N_{\mathrm{I}} = 100$ vectors, where each population vector has the format given in (8) and whose entries are generated uniformly over the allowable range. The fitness function is computed for the initial population, and the best $N_{\mathrm{B}} = 10$ vectors (those with the highest fitness) are retained.

The GA uses N_{B} population vectors to generate $N_{\mathrm{GA}} = 60$ new population vectors using mutations and cross-overs, where cross-overs are only possible within the same parameter type (e.g. source voltages with source voltages), and the mutation probability is varied from 10% to 50%. The fitness function is evaluated for N_{GA} population vectors and only the best N_{B} vectors are retained.

The steps in the previous paragraph are repeated $N_{\mathrm{R}} = 100$ times and the vector in the final population having the highest fitness is declared to be the solution.

C. Rician Fading Example

As an example, we have considered synthesizing a Rician distribution given by

$$f(x|\nu,\sigma) = \frac{x}{\sigma^2}\exp\left[-\frac{(x^2+\nu^2)}{2\sigma^2}\right] I_0\left(\frac{x\nu}{\sigma^2}\right), \qquad (10)$$

where I_0 is the modified Bessel function of the first kind with order zero. In our simulations, we optimize ERRC parameters for a few different values of σ for a constant value of ν. For fitness computations, the actual pdf for a single parameter vector $\mathbf{w}$ is obtained using 10^4 random realizations of the RE loads and computing a histogram.

Figure 6 plots the Rician probability distribution function (pdf) obtained using (10) and the optimal solution from the GA, where the field was sampled at the center of the chamber. As can be seen, a very close fit to the desired distribution can be obtained by proper selection of the RE parameters.

D. Frequency Selective Fading

Previous sections have demonstrated that the ERRC is capable of providing useful fading distributions at a single frequency. However, due to the small size of the chamber, one may question whether useful frequency-selective fading is possible. To provide frequency selectivity, the chamber must reverberate, or in other words, the signal transmitted from a source port must be involved in multiple bounces in the chamber before decaying to a negligible level.

In order to analyze the frequency response characteristics of the field generated inside the chamber, we have simulated the structure from 280 to 320 MHz, where the chamber diameter is 4 m (or 4λ at 300 MHz). The control parameters used in this case are the ones that generated the Rayleigh amplitude distribution in the first example. Figure 7 plots the field power in dB at the center of the chamber versus frequency for 4 random realizations of RE reactances. As is evident, significant and diverse frequency selectivity is obtained for the different random states.

E. Channel Delay Spread

One potential application of the ERRC is to produce a certain delay spread of multipath to simulate a specific wireless channel. Here we illustrate the delay spread obtained for a single set of parameters, suggesting that delay-spread optimization is also possible using the optimization techniques described previously. In this study we again use 10^4 random realizations of RE impedance states, where for each realization we compute the frequency-dependent field $E_z(f)$ at the center of the chamber and the associated time-domain response $E_z(t)$ using an inverse Fourier transform. The mean power of the frequency- and time-domain responses is computed by averaging $|E_z(f)|^2$ and $|E_z(t)|^2$ respectively over the 10^4 realizations.

Figure 8 plots the average frequency- and time-domain power over the 40 MHz bandwidth. Both plots are normalized to obtain a maximum value of 1 (0 dB). The frequency step size was chosen to be 0.25 MHz, which corresponds to a

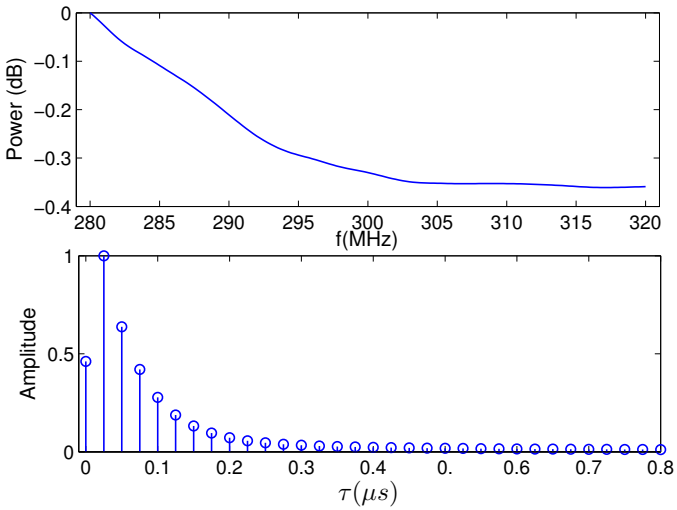

Fig. 8. Average frequency- and time-domain power at the center of the ERRC over a bandwidth of 40 MHz.

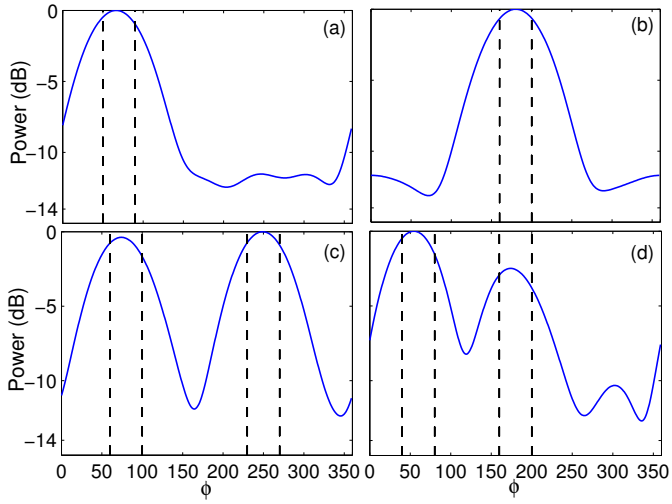

Fig. 9. Dependence of propagating power versus arrival angle ϕ generated for various desired directional profiles. The sectors where propagation is desired in each case is denoted by the dashed boxes.

maximum unambiguous delay of 4 μs. Since 161 points are used to cover 40 MHz bandwidth, the time resolution is 25 ns. The results demonstrate that the average power delivered to each frequency is fairly constant and that the average delay spread is on the order of 150 ns. Note that the time for a propagating wave to travel the width of the chamber (4 m) is 13 ns, which indicates a useful level of reverberation. As stated previously, more precise control of the delay spread is likely to be possible using optimization techniques.

F. Directional Propagation Characteristics

Another potential application of the chamber is to generate multipath with a certain power angle spectrum (PAS). For example, in many wireless propagation environments, multipath tend to come in clusters, and one may desire to specify a PAS composed of one or more such clusters. In order to explore the idea of generating different PAS profiles, fields inside the chamber can be transformed from element space into wavenumber (or propagation direction) space using the equation

$$S(\phi) = \int_A E(x,y) \exp[-jk_0(x\cos\phi + y\sin\phi)]\, dA, \quad (11)$$

where the two-dimensional integral is performed over the circular area A having a diameter of $\lambda/3$ positioned at the center of the chamber.

In this initial test, we obtain a desired directional profile by first generating a library of solutions as follows. Source voltages and resistances are fixed as $\mathbf{v}_s = [1 \;\; j \;\; -1 \;\; -j]^T$ and $R_i = 37\ \Omega$, respectively. A set of 100 pairs of $X_{\min}$ and $X_{\max}$ are generated with $X_{\min} \sim \mathcal{U}(-2\eta_0, 2\eta_0)$ and $X_{\max} \sim \mathcal{U}(X_{\min}, 2\eta_0)$. For each pair of $X_{\min}$ and $X_{\max}$, 10^4 realizations of the loads are generated, where $X_i \sim \mathcal{U}(X_{\min}, X_{\max})$. This process results in a library of 10^6 random solutions. For a desired directional profile, the best 10^3 solutions from the library that produce propagation in the desired directions are kept and replayed to simulate fading with the desired directional bias.

Figure 9 illustrates that the library of solutions contains useful and diverse directional profiles, where for each case we have specified sectors of desired receive power (dashed lines) and have plotted the average power over the best 10^3 solutions. This simple example illustrates that even without detailed optimization, useful directional properties of the wave field can be controlled.

V. Conclusion

This work has explored the idea of an electronically reconfigurable reverberation chamber (ERRC) whose purpose is to allow realistic OTA testing of wireless devices in a cost effective way. This initial study of an idealized two-dimensional chamber suggests that such chambers may allow fading distribution, spatial correlation, frequency selectivity, and directional bias of different multipath channels to be simulated. Future extensions of this work are to perform an analysis of a three dimensional chamber and develop practical ERRC implementations.

References

[1] Wei Fan, X. C. B. de Lisbona, Fan Sun, J. O. Nielsen, M. B. Knudsen, and G. F. Pedersen, "Emulating spatial characteristics of MIMO channels for OTA testing," *IEEE Transactions on Antennas and Propagation*, vol. 61, no. 8, pp. 4306–4314, 2013.

[2] A. Scannavini, L. J. Foged, M. Anouar, N. Gross, and J. Estrada, "OTA throughput measurements by using spatial fading emulation technique," in *Proceedings of the Fourth European Conference on Antennas and Propagation (EuCAP'10)*, Barcelona, Spain, Apr. 12-16, 2010, pp. 1–5.

[3] P. Kyösti, J.-P Nuutinen, and T. Jamsa, "MIMO OTA test concept with experimental and simulated verification," in *Proceedings of the Fourth European Conference on Antennas and Propagation (EuCAP'10)*, 2010, pp. 1–5.

[4] P-S. Kildal, C. Orlenius, and J. Carlsson, "OTA testing in multipath of antennas and wireless devices with MIMO and OFDM," *Proceedings of the IEEE*, vol. 100, no. 7, pp. 2145–2157, 2012.

[5] M. A. Garcia-Fernandez, J. D. Sanchez-Heredia, A. M. Martinez-Gonzalez, D. A. Sanchez-Hernandez, and J. F. Valenzuela-Valdes, "Advances in mode-stirred reverberation chambers for wireless communication performance evaluation," *IEEE Communications Magazine*, vol. 49, no. 7, pp. 140–147, 2011.

[6] A. M. Eid and J. W. Wallace, "Accurate modeling of body area network channels using surface-based method of moments," *IEEE Transactions on Antennas and Propagation*, vol. 59, no. 8, pp. 3022–3030, 2011.